LASER & PHOTONICS REVIEWS

Laser Photonics Rev. **10,** No. 4, 612–622 (2016) / **DOI** 10.1002/lpor.201500332

ORIGINAL PAPER

Abstract III-nitride light-emitting diodes (LEDs) and laser diodes (LDs) are ultimately limited in performance due to parasitic Auger recombination. For LEDs, the consequences are poor efficiencies at high current densities; for LDs, the consequences are high thresholds and limited efficiencies. Here, we present arguments for III-nitride quantum dots (QDs) as active regions for both LEDs and LDs, to circumvent Auger recombination and achieve efficiencies at higher current densities that are not possible with quantum wells. QD-based LDs achieve gain and thresholds at lower carrier densities before Auger recombination becomes appreciable. QD-based LEDs achieve higher efficiencies at higher currents because of higher spontaneous emission rates and reduced Auger recombination. The technical challenge is to control the size distribution and volume of the QDs to realize these benefits. If constructed properly, III-nitride light-emitting devices with QD active regions have the potential to outperform quantum well light-emitting devices, and enable an era of ultra-efficient solid-state lighting.

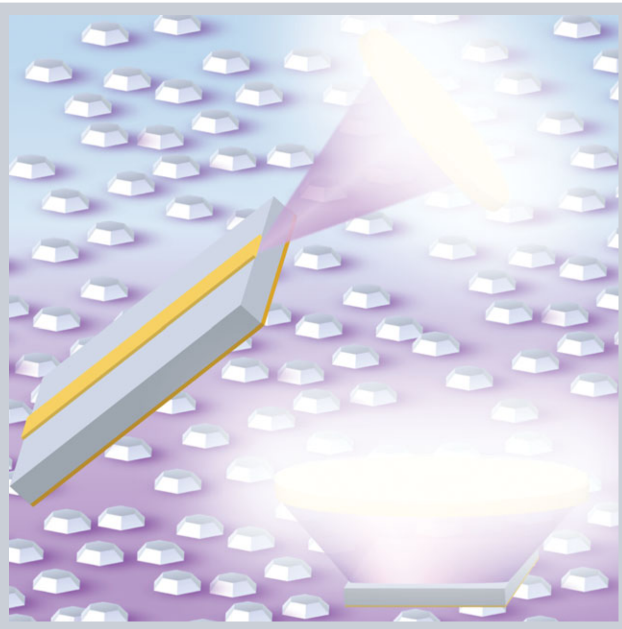

III-nitride quantum dots for ultra-efficient solid-state lighting

Jonathan J. Wierer Jr.[1,*], Nelson Tansu[1], Arthur J. Fischer[2], and Jeffrey Y. Tsao[2]

1. Introduction

III-nitride light-emitting diodes (LEDs) have achieved impressive efficiencies with peak power conversion efficiencies (PCEs) of ∼ 84% [1]. As manufacturing volumes have increased they are becoming cost competitive with traditional lighting technologies [2, 3]. However, Auger recombination causes a phenomennon called "efficiency droop" where the radiative efficiency of III-nitride quantum well (QW) LEDs decreases with increased current [4–7], and consequently limits the peak PCE to low current densities (< 10 A/cm^2). The most effective method, to date, to mitigate efficiency droop is to shift the onset to higher currents by lowering the carrier density at a particular operating current. For a roughly fixed areal chip cost, LEDs operated at low current densities will produce fewer lumens per unit chip cost, hence there is tremendous economic incentive to mitigate Auger recombination and efficiency droop [8]. The current stopgap solutions all involve decreasing carrier density at a particular operating current by increasing active volume, but they all have fundamental limitations. For example, device emitting area can be increased [9], but this increases the cost per LED. Or, for example, the thickness [10–12] or number of QWs can be increased [13, 14], but short carrier diffusion lengths limit the carrier filling uniformity. The unfortunate reality is that, despite much effort, QW-based III-nitride LEDs are still only very efficient at lower current densities. Therefore, to further advance solid-state lighting (SSL) efficiency other (non-QW) solutions may be necessary.

III-nitride laser diodes (LDs) have also achieved impressive peak PCEs of ∼40% [15–17], and are gaining interest as an alternative source for SSL. They have many attributes that make them interesting for SSL [8, 18] including system and cost benefits [2, 18] and an ability for phosphor-converted LDs (pc-LDs) to produce white light with the same color rendering and color temperature as pc-LEDs [19–22]. Most interesting, in contrast to LEDs, LD operate under stimulated emission after lasing threshold, and parasitic recombination processes such as Auger are clamped at threshold. The result is III-nitride LDs have higher PCEs at much higher current densities than LEDs, and are a potential way to overcome efficiency droop [8]. Indeed, projections of the efficiency of QW-based LDs suggest they could achieve peak PCEs of ∼70% which vastly exceed those of LEDs at high current densities [8]. However, peak PCEs of LDs are not as high as the 84% peak PCEs of LEDs, in large part because high thresholds from Auger recombination results in a peak PCE at very high

[1] Lehigh University, Department of Electrical and Computer Engineering, Center for Photonics and Nanoelectronics, Bethlehem, PA 18015
[2] Sandia National Laboratories, Albuquerque, NM 87185
*Corresponding author: e-mail: jwierer@lehigh.edu

© 2016 by WILEY-VCH Verlag GmbH & Co. KGaA, Weinheim

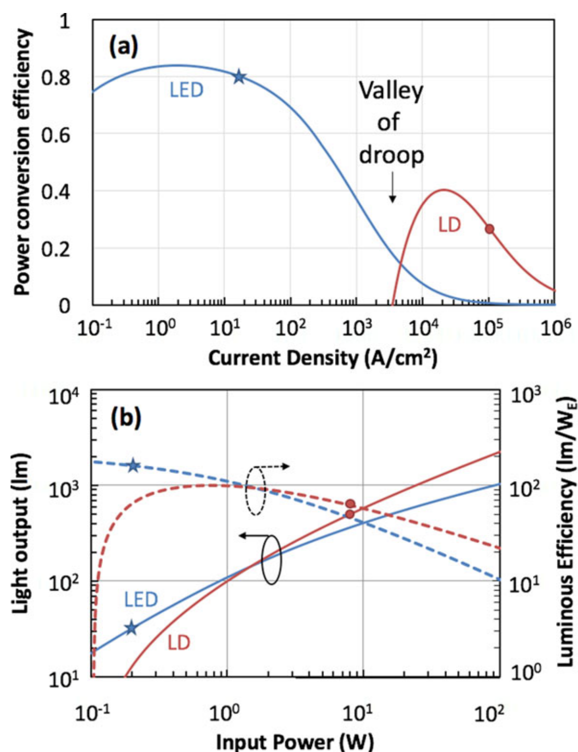

Figure 1 Plot of (a) power conversion efficiency (PCE) vs. current density for a state-of-the-art (SOTA) LED [1] and LD [15] emitting at violet wavelengths. Plot of (b) the light output in lumens and luminous efficiency (lm/W_E) vs. input power for the same two devices. At current densities of 10^3 – 10^4 A/cm^2 is the valley of droop. The blue stars highlight standard operating conditions of the LED, and the red circles are for a 500 lm pc-LD. Note that while the peak PCEs are far apart in (a) the peak lm/W_E are much closer in (b) because of the input power scale and larger LED area (43 times).

current densities (kA/cm^2) where parasitic electrical resistive loss become substantial.

In other words, Auger recombination not only limits LED performance, but also LD performance. To illustrate this further, Fig. 1a shows PCE versus current density for a state-of-the-art (SOTA) LED [1], and SOTA LD [15] both emitting at violet (405-415 nm) wavelengths. For LEDs, Auger recombination grows super-linearly with increased current density and dominates at high currents, relegating the peak PCE to low current densities (<10 A/cm^2). For LDs, Auger recombination becomes an appreciable fraction of the total current near threshold, causing a high threshold current density and high parasitic resistive losses, which in turn limits the peak PCEs of the LD. Between the PCE peaks is the valley of droop at mid-range current densities where both emitters are inefficient.

The different LD and LED PCE characteristics present different challenges when designing a SSL-grade white-emitting source that can produce 500 lm or more. To demonstrate these challenges, Fig. 1b shows the light output (lumens) and luminous efficiency (output lumens over electrical input power, lm/W_E) versus input power of phosphor-converted versions of the LED and LD in Fig. 1a. Only a single LED and LD is shown and other device details are given in Table 1. Also a simple "effective" phosphor and package efficiency of 250 lm/W (lumens of final white light produced per Watt of violet emitted) is used.

The SOTA LED [1] is typically operated at ~150 A/cm^2 or input powers of ~0.2 W, in order to have high luminous efficiencies of ~160 lm/W_E (blue stars, Fig 1). This produces only ~32 lm, and this is not enough for a single SSL-grade source. There are two options to remedy this problem. The first is to increase the number of LEDs. This is done in practice by the authors in Ref. 1, and 15 of them are connected in a series/parallel configuration to provide ~500 lm. Increasing the area of the chip is a similar tactic and also used [23, 24], however, both increase costs. The second option is to drive a single LED at higher input powers. This aids in limiting costs, but Fig. 1b shows the lm/W_E falls to unacceptable levels as the input power is increased. The peaking of LED PCE at low input power densities causes this luminous efficacy (lm/W_E) versus cost tradeoff. Shifting the peak PCE to higher input powers is critical for the advancement of LEDs for SSL.

In contrast, the SOTA LD [15] operates more efficiently at higher input powers. The pc-LD would produce ~500 lm at 8.2 W (1.2×10^5 A/cm^2), but only have a luminous efficiency of ~60 lm/W_E (red circles, Fig. 1). Adding more LDs and operating at lower input powers would only increase cost and marginally improve luminous efficiency. The SOTA LDs peak PCE is too low to compete with the LED operated at low input powers, and there is a need to increase peak PCEs of LDs for SSL.

Clearly, for both LD and LEDs, we need to improve efficiencies at the valley of droop or higher currents to further advance SSL. Transformational methods will need to be found to address the limitations imposed by Auger recombination. One possible approach is to use a new type of active region in III-nitrides to achieve drastic reductions in threshold carrier densities and increases in spontaneous emission rates. Such improvements are essential to improve higher current performance in both LEDs and LDs.

It has been recognized for some time that quantum dots (QDs) have benefits over QWs. For LDs, QDs can be used to achieve lower threshold currents due to higher gain and lower threshold carrier densities [25, 26]. For LEDs, the QDs higher spontaneous emission will counteract Auger recombination, and additionally there is experimental and theoretical evidence that QDs should have suppressed or completely inhibited Auger recombination [27–29]. QD active regions in LDs and LEDs could lead to more efficient sources in the valley of the droop and higher currents. While there has been some work on InGaN QDs with some impressive results [29–34], it is not clear what ultimate device efficiencies could be achieved using InGaN QDs in both LEDs and LDs.

In this paper, we explore InGaN QD active layers in both LEDs and LDs to determine their impact on efficiency. This paper is a corollary to Ref. 8, that compares LDs

© 2016 by WILEY-VCH Verlag GmbH & Co. KGaA, Weinheim

Table 1 Physical parameters for calculating LED and LD efficiencies. For some parameters two values are given either original/improved or small/large. Parameters left blank are not used

Grouping	Parameter	Parameter Description	Quantum Well LED	Quantum Well LD	Quantum Dot LED	Quantum Dot LD
Structural	A_d (cm^{-2})	Device area	3.9×10^{-4}	9×10^{-6}	3.9×10^{-4}	9×10^{-6}
	t (nm)	layer thickness	10	2.5	2.4	2.4
	N_l	Number of layers	10	3	20	6
	In	In concentration	-	-	0.27	0.27
	λ *(nm)*	Wavelength	415	407	405	405
	BW (nm)	QD base width	-	-	4	4/9 (small/large)
	BD (nm)	QD base depth	-	-	4.62	4.62/10.4 (small/large)
	FF	QD Fill Factor	-	-	.01	.01
Radiative and injection efficiency	*A* (1/s)	SRH recombination coefficient	2.2×10^{5}	2.2×10^{5}	2.2×10^{5}	2.2×10^{5}
	B_o(cm^3/s)	Radiative recombination constant	1.45×10^{-11}	1.36×10^{-10}	-	-
	C_o(cm^6/s)	Auger recombination constant	1×10^{-30}	2.34×10^{-30}	2.34×10^{-30}	2.34×10^{-30}
	n^*(1/cm^3)	Carrier density fitting parameter	3.8×10^{18}	6×10^{18}	6×10^{18}	6×10^{18}
	η_{inj}	Injection efficiency	0.95	0.95	0.95	0.95
Optical gain	ΔE_{inh} *(meV)*	Inhomogenous broadening	-	-	5	5
	ΔE_h *(meV)*	Homogenous broadening	-	-	25	25
	Γ	Confinement factor, transverse	-	0.27 / 0.135 (orig./imp.)	-	0.24
	N_{0D} *or* N_{2D} $(1/cm^3)$	Effective density of states	7.9×10^{18}	7.9×10^{18}	6.01×10^{17}	6.01×10^{17}
	N_{tr} (1/cm^3)	Transparency current density	-	2.31×10^{19}	-	2.31×10^{17}
	G_0 (cm^{-2})	Differential gain	-	1.17×10^{-16}	-	6.4×10^{-15}
Extraction efficiency	α_I (1/cm)	Internal loss	-	12 /1.2 (orig./imp.)	-	1.2
	α_m (1/cm)	Mirror loss	-	27.7	-	14.45
	η_{ext}	Extraction efficiency	0.9	-	0.9	-
Joule Efficiency	$R_{s,}$ (ohms)	Series resistance	2.9	4 / 0.8 (orig./imp.)	2.9	0.8
	I_o (A)	Reverse saturation current	1×10^{-27}	5×10^{-25}	1×10^{-27}	5×10^{-25}
	$n_{f,}$	Ideality factor	1.5	2	1.5	2

and LEDs for SSL, except here we incorporate InGaN QD active layers along with our best current understanding of InGaN QD optical physics. First, we investigate QDs as active layers for LDs to reduce threshold and peak PCE current densities. A properly constructed InGaN QD active layer greatly reduces the transparency carrier density and, with high enough differential gain, avoids appreciable Auger recombination. Second, we investigate InGaN QDs in LEDs to overcome efficiency droop. Properly formed InGaN QDs leads to higher spontaneous emission and lower Auger recombination.

Throughout the paper, to determine possible phosphor-converted white LED and LD PCEs and light output, we use a simple "effective" phosphor and package efficiency of 250 lm/W. We conclude that the use of QDs in both LEDs and LDs has the potential to lead to record peak PCEs at higher current densities and hence at high white lumen output per unit cost. The key to realizing these improvements,

© 2016 by WILEY-VCH Verlag GmbH & Co. KGaA, Weinheim

however, is to develop synthesis methods to form QDs with the appropriate volume and size distribution. The ultimate goal of this work is to stimulate deeper investigation of InGaN QDs as a means to overcome Auger losses and enable ultra-efficient SSL.

2. Theory of laser diodes with InGaN quantum dots

When designing an emitter for SSL, the goal is to maximize the PCE (or wallplug efficiency) which is defined as the extracted optical watts per input power. The PCE of the LD ($\eta_{PCE,LD}$) can be expressed as four different efficiencies:

$$\eta_{PCE,LD} = \eta_J \ \eta_{inj} \ \eta_{stim} \ \eta_{ext}, \tag{1}$$

where η_J is the joule efficiency, η_{inj} the injection efficiency, the η_{stim} stimulated efficiency, and η_{ext} the extraction efficiency. The equations for the four individual efficiencies and the parameters that affect them are detailed in Ref. 8.

To illustrate how these individual efficiencies, affect the PCE we plot in Fig. 2a the efficiencies versus current density of a SOTA violet LD (same as Fig. 1) [15]. The four efficiencies behave in different ways with respect to current density. The η_{inj} for a LD operating above threshold can be assumed to be constant with current density, attributed to the carrier clamping at threshold [35]. The η_{ext}, in general is also constant with current density. On the other hand, the η_{stim} and η_J are not constant and oppose one another. The η_J is high at low currents and decreases with increasing current as resistive losses increase. The η_{stim}, however, increases from zero after threshold, and then asymptotes to a maximum. Unfortunately, high η_{stim} occurs only after resistive losses become a problem.

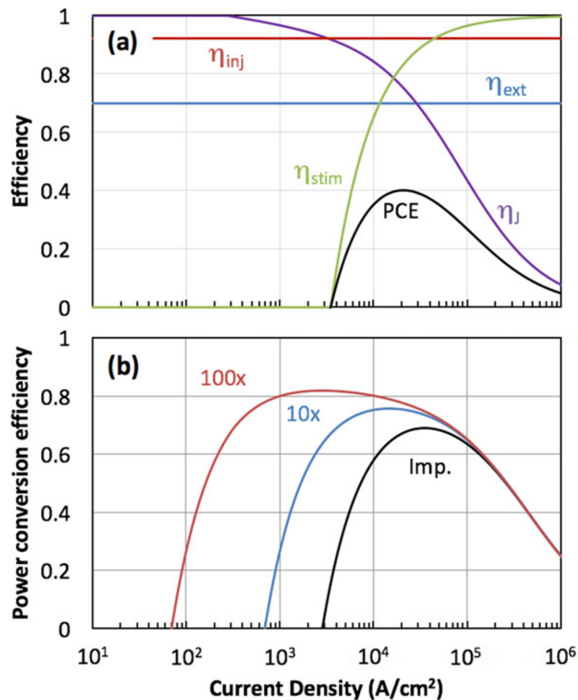

Figure 2 Plot of (a) efficiencies vs. current density for a state-of-the-art (SOTA) LD [15]. Plot of (b) power conversion efficiency vs. current density of an improved (Imp.) LD, a LD with 10 times (10x), and 100 times (100x) change in threshold carrier density (N_{tr}) and spontaneous emission rate (BN^2). The N_{tr} is higher while the BN^2 is lower. The improved LD has a reduced resistance and optical loss, and increased confinement. The lower N_{tr} greatly reduces the threshold current and increases peak power conversion efficiency.

These two latter efficiencies thus define and bound the shape of the PCE versus current density curve. And, because the η_{stim} increases only after resistive losses become a problem, lowering the threshold current density or decreasing the resistive losses would lead to dramatic increases in PCE. Possible improvements to LDs with a QW-based active region were analyzed in great detail in Ref. 8. Using this analysis, the black line in Fig. 2b shows the PCE versus current density for a QW-based LD with improvements of 5 times for resistance and confinement factor, and 10 times for optical loss. There is a marked improvement in the peak PCE to ~70%. While a significant improvement, since threshold current densities have only been slightly reduced, it is ultimately still limited by resistive loss. For more dramatic reductions in thresholds and increases in PCE at lower currents, another path needs to be taken.

One such alternative path is to change the recombination physics within the active layer. This can be illustrated using the phenomenological expression for threshold current density, J_{th}, in a LD [36]:

$$J_{th} = \left(\frac{qt}{\eta_{inj}}\right) \left[AN_{th} + BN_{th}^2 + CN_{th}^3\right], \tag{2}$$

where t is the active layer thickness, A is the defect (Shockley-Read-Hall) recombination coefficient, B the spontaneous emission recombination coefficient, C the Auger coefficient, and N_{th} the threshold carrier density. Normally, this expression is simplified so spontaneous emission is the dominant factor in J_{th}. However, the large Auger recombination in III-nitrides requires us to also include the CN_{th}^3 term which accounts for approximately half J_{th} in blue LDs [8]. Keeping this in mind, to lower J_{th} we need to not only lower the spontaneous emission rate at threshold, ${BN_{th}}^2$, but also the Auger recombination rate at threshold, ${CN_{th}}^3$. These rates are ultimately determined by bandstructure and electronic states. A lowering of the spontaneous emission rate is illustrated in Fig. 2b where we arbitrarily lower N_{th} and increase B concurrently by 10 times (blue line) and 100 times (red line). These changes in N_{th} and B are expected with QD active layers, as will be discussed further. The net result is a reduction in BN_{th}^2 and dramatic reduction in the current densities at threshold and at peak PCE.

The A coefficient is also included in the model, but in state-of-the-art LEDs and LDs the AN term has become much smaller compared to the other two terms

© 2016 by WILEY-VCH Verlag GmbH & Co. KGaA, Weinheim

(BN^2 and CN^3). This is especially true when modeling the state-of-the-art LED and LD shown in Fig. 1. Both use $A = 2.2\times10^5$ s^{-1}, and the value is so small that it has little effect on the threshold currents or peak power conversion efficiencies. One could increase the A coefficient to see a larger effect, however the goal in this paper is to determine ultra-efficiency and use best-case values.

While this exercise of lowering the J_{th} is quantitatively interesting we need to determine the magnitude of these changes with QDs. To accomplish this let us take a closer look at the gain of the QDs which is a determining factor of N_{th}. For InGaN materials the peak gain, g, at a particular wavelength can be approximated by a linear function [37]:

$$g = G_0 \; (N - N_{tr}) \tag{3}$$

where G_0 is the differential gain (dg/dN), N is the carrier density, and N_{tr} is the transparency carrier density. Transparency is achieved when the quasi-Fermi levels are separated enough to create population inversion (Bernard-Duraffourg Condition). At threshold, the gain equals the total losses, α, and:

$$N_{th} = \frac{\alpha}{G_0} + N_{tr}. \tag{4}$$

Eqn. (4) shows that to decrease the threshold carrier density we need to lower the transparency carrier density or increase differential gain. These equations so far show that when designing a low threshold LD, what is critical is high G_0, low losses, and low N_{tr}. The advantages of higher G_0 and lower N_{tr} can be achieved with QDs.

The first advantage of QDs is higher differential gain. To determine G_0 we use the gain spectra, $g(h\nu)$, expressed as:

$$g(h\nu) \propto \sum_n \int_0^\infty \rho_r(E)\left[f_c(E) - f_v(E)\right] dE \tag{5}$$

where, $\rho_r(E)$ is the density of states, f_c is the conduction band occupation probability, f_v the valence band occupation probability, and n is the quantum state number. The advantage of a QD active region is manifest in the density of states. The density of states for a QW is step-like versus energy, while density of states for the QD is a delta-like [38]. For ideal QDs, carriers are fed into nearly identical energy states which leads to an increase of G_0. This increased G_0 will lower threshold carrier density (Eqn. (4)).

The second advantage for QDs is the transparent carrier density, which is much lower compared to the QWs at the same quasi-Fermi separation and energy transitions. The carrier concentration for a QW, N_{QW} is [38]:

$$N_{QW} = N_{2D} \sum_n ln\left(1 + e^{(E_{fc} - E_n)/kT}\right) \tag{6}$$

where E_{fc} is the quasi-Fermi level in the conduction band, E_n is the energy of the n$^{\text{th}}$ state, and N_{2D} is the effective density of states for a QW. The carrier concentration for a QD, N_{QD}, is much different, and can be expressed as [38]:

$$N_{QD} = 2N_{0D} \sum_{m,n,l} \int_0^\infty G(E)\, f_c(E)\, dE \tag{7}$$

where $G(E)$ is a Gaussian function representing the inhomogeneous broadening (QD energy distribution from varying sizes), m, n, and l are the quantum state numbers, and N_{0D} is the effective density of states for a QD. (The equations for hole concentration are similar). When comparing Eqns. (6) and (7) the magnitude of the carrier density is largely determined by the effective density of states. For InGaN QWs it is N_{2D} $\sim10^{19}$ /cm^3,while for QDs it is N_{0D} $\sim10^{17}$ /cm^3 for our chosen QD densities and thicknesses (see Table 1). Of course, the size of the QDs needs to be small to control the number of quantum states and ultimate carrier density For ideal QDs that are small (limited quantum states) and have low inhomogeneous broadening the result is extremely low threshold carrier densities.

We should note there is also a third advantage in wavefunction overlap for QDs. Overlap is contained within the gain expression, and we estimate it is $\sim$0.15 and $\sim$0.5 for an unscreened QW and small-sized QD emitting at $\sim$407 nm, respectively. These values are for fully strained QDs, and some partial strain relaxation (not considered here) would lead to higher overlap. Increased overlap not only increases gain, but also spontaneous emission rate.

There is also an increase in the spontaneous emission rate for QDs. This is advantageous for LEDs, but for LDs it is a parasitic recombination process that increases threshold. The $BN_{th}{}^2$ term in Eqn. (2) can be replaced with the total spontaneous emission rate at threshold, R_{sp}^{th}, determined the following way. The gain spectra and spontaneous emission spectra, R_{sp}, are related by [38]:

$$R_{sp}(h\nu) = \frac{n^2\omega^2}{\pi^2\hbar c^2}\,\frac{f_c(1 - f_v)}{(f_c - f_v)}\, g(h\nu) \tag{8}$$

where n is the optical index, and ω is the angular frequency. Integration of R_{sp} over all energies at the threshold carrier density gives R_{sp}^{th}. Therefore, we can use the gain spectra to also determine the R_{sp}^{th} in the QDs.

The equations and properties described above are well known from extensive and impressive QD research [25,26, 39–42], and not intended to be presented as new. The goal of this section (and for modeling LEDs in section 4) is to present some theoretical background to give the reader a foundational understanding of the benefits of InGaN QD active layers and how they apply to designing light-emitting devices.

To perform the calculations below, we used a similar approach as Ref. 8, using the additional equations presented above, and the parameters listed in Table 1. The active layers are formed on the c-plane of GaN, and have barrier layers of GaN. The QDs are shaped as hexagonal pyramids, have $\{10\bar{1}1\}$ side facets, and the base of the pyramid is larger than the top. To determine bandstructure and

© 2016 by WILEY-VCH Verlag GmbH & Co. KGaA, Weinheim

quantum states, effective masses for electrons and holes are inputted into a 3-dimensional Schrodinger-Poisson solver [43]. Many body effects, excitons, and strain relaxation are not considered in this analysis. However, we would expect higher performance, such as higher gain when including many body effects [33], if these were included.

3. Efficiencies of InGaN QD-based laser diodes

We now compare the gain of a QD and QW active layer. Fig. 3a shows the gain spectra versus energy for a single QW and single layers of QDs at carrier densities greater than N_{th}. Two different sizes of QDs are shown, labeled small and large, and the dimensions of the QDs are given in Table 1. For the QWs and QDs the homogeneous broadening is 25 meV [44], and the inhomogeneous broadening for the QDs is 5 meV. While this inhomogeneous broadening is small, we will show it is necessary to achieve the ultimate improvement in threshold currents and PCE. The density of states for the QDs results in narrower gain spectra. For the large QDs the gain is shared with the many quantum states at multiple energies, while for the small QDs, the second energy transition is further away in energy and most of the carriers and gain is present in the lowest energy transition at the given carrier density.

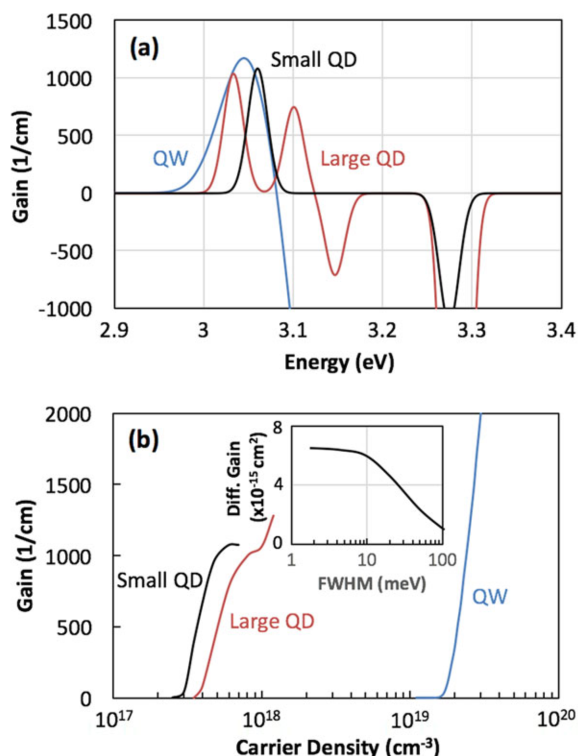

Figure 3 Plot of (a) gain spectra for a single QW at $N = 2.5\times10^{19}$ cm^{-3} (blue line), a layer of large QDs at $N = 9\times10^{17}$ cm^{-3} (red line), and a layer of small QDs at $N = 7\times10^{17}$ cm^{-3} (black line). Plot of (b) peak gain vs. carrier density for a single QW, a layer of large QDs, and layer of small QDs. Inset plots the differential gain of the small QDs vs. the full-width at half maximum (FWHM) of the inhomogeneous broadening energy.

As discussed above, the QD has a profound effect on G_0 and N_{tr} resulting in a lower threshold carrier density. Fig. 3b shows the peak gain of a single QW and single layers of QDs versus carrier density. The QD layers have nearly two orders of magnitude lower N_{tr} than the QW. While the large QDs have low N_{tr}, the G_0 is less than the small QDs because of the additional quantum states. To illustrate how dramatically different N_{th} and G_0 are, if we assume a threshold modal gain of 1000 cm^{-1}, the QW would have $N_{th} = 2.4\times10^{19}$ cm^{-3} and $G_0 = 1.5\times10^{-16} cm^2$, and the QD would have $N_{th} = 5.5\times10^{17}$ cm^{-3} and $G_0 = 6.5\times10^{-15} cm^2$. Therefore, we should expect a large decrease in threshold currents for QDs layers. It should be noted that the QDs saturate due to the limited number of quantum states. Therefore, to achieve enough gain either more than one QD layer or a larger QD density is required. The large QDs exhibit a saturation, followed by an increase in gain caused by the filling of the second favorable energy transition.

Up till now we have only considered low (5 meV) inhomogeneous broadening. The impact on differential gain on the full-width at half-maximum (FHWM) of the inhomogeneous broadening for the small quantum dots is shown in the inset of Fig. 3b. As the FWHM increases the differential gain decreases. There is steep drop-off in differential gain at ~10 meV, and the differential gain at 5 meV is 7 times larger than at 100 meV. This translates into a 7 times difference in the threshold carrier density. This plot illustrates how critical it is to control the inhomogeneous broadening within the QD layers.

The lower threshold carrier densities of the QDs have a big impact on the PCE. Fig. 4a shows the PCE versus current density for a QD-based LD with 6 layers of small QDs at a density of $\sim7.2\times10^{10}$ cm^2. The SOTA QW-based LED (from Fig. 1a) and improved QW-based LD (from Fig. 2b) are included for comparison. The threshold current density of the QD LD is ~170 A/cm^2, over an order of magnitude lower than the improved QW-based LD. The peak PCE is ~80% at ~5.7 kA/cm^2 which is a much lower current density for peak PCE and rivals the peak PCE of the LED. The large reduction of threshold currents goes a long way to filling the valley of droop.

Fig. 4b shows the light output (lumens) and luminous efficiency (lm/W_E) versus input power from these sources. The peak luminous efficiency of the QD-based LD is at an input power of 0.2 W, similar to the operating currents of the STOA LED, but provides ~40 lm compared to ~32 lm for the LED. More interesting is at an input power of 3 W the QD-based LD has an output power of ~500 lm and a luminous efficiency of 165 lm/W_E. This luminous efficiency is approximately the same as the LED operated at an input power of 0.2 W, but this single LD achieves the 500 lumens needed for SSL-grade source. However, the advantage of the QD active layer decreases as the QW-based LD performance converges at higher input powers. This convergence is due to resistance that dominates for both at higher current densities. If such performance can

© 2016 by WILEY-VCH Verlag GmbH & Co. KGaA, Weinheim

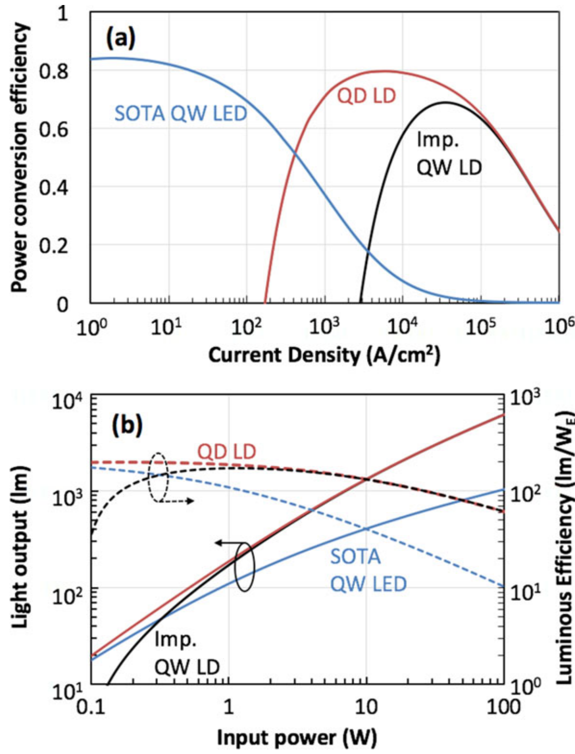

Figure 4 Plot of (a) power conversion efficiency vs. current density of a state-of-the-art (SOTA), QW-based LED (blue line), an improved QW-based LD (black line), and a QD-based LD (red line). The QD LD has extremely low threshold currents and peak efficiencies that rival the QW-based LED. Plot of (b) light output in lumens and luminous efficiency (lm/W_E) vs. input power for the three emitters in (a). The QD LD has higher light output for all input powers.

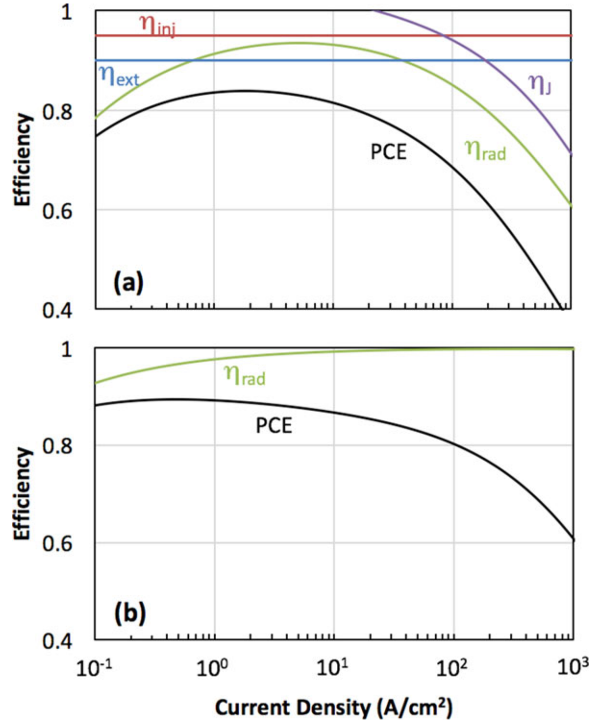

Figure 5 Plot of efficiencies vs. carrier density for (a) a state-of-the-art (SOTA) QW-based LED, and (b) a QW LED with an increase in spontaneous emission rate and reduction of Auger recombination rate by 10 times. The radiative and joule efficiency dominate the power conversion efficiency (PCE) at high carrier current densities. The improvements in the spontaneous and Auger recombination rates lead to higher PCE at high current densities.

be achieved, then additional steps will need to be taken to reduce resistances for further improvements.

4. Theory of light-emitting diodes with InGaN quantum dots

To model the PCE of LEDs we use a similar methodology. The PCE for LEDs, $\eta_{PCE,LD}$, can also be separated into four different efficiencies [8]:

$$\eta_{PCE,LED} = \eta_J \ \eta_{inj}\eta_{rad}\eta_{ext}, \tag{9}$$

where η_{rad} is the radiative efficiency. While the subscripts of the other three efficiencies are identical to the LD, the expressions can be different. The equations for the individual efficiencies and the parameters that affect them are detailed in Ref. 8.

To illustrate how these individual efficiencies affect the PCE we plot in Fig. 5a the efficiencies versus current density of a the SOTA LED [1]. Just like the LD, the η_{ext} is approximately constant with current density. The η_{inj} can have a dependency on current density [45], but this value is relatively high at low operating current densities for optimized structures. In the present analysis, we have assumed a constant η_{inj} versus current density by assuming an optimized heterostructure design. The η_{rad} and η_J, on the other hand, decrease as the current density increases. For η_J, the culprit is resistive losses which increases as the current density increases. The η_{rad} also decreases with current density due to a rapid increase in Auger recombination. These two efficiencies cause the decrease in $\eta_{PCE,LD}$ with increasing current. Reducing resistances and improving radiative efficiencies will lead to improved PCE at higher currents. Here, we concentrate on how the η_{rad} can be dramatically improved by employing QDs.

To change the radiative efficiency of an LED we need to affect the recombination physics within the active layer. The radiative efficiency of an LED can be phenomenologically expressed as:

$$\eta_{rad} = \frac{BN^2}{AN + BN^2 + CN^3}. \tag{10}$$

The AN, BN^2, and CN^3 terms are approximations of Shockley-Read-Hall, spontaneous emission, and Auger recombination rates, and in reality, these rates can stray from their constant power dependencies. One way to approximate this change is to express the coefficients

© 2016 by WILEY-VCH Verlag GmbH & Co. KGaA, Weinheim

as functions of N [46]. For example, C could be expressed as:

$$C = \frac{C_0}{1 + N/N^*} \tag{11}$$

where N^* is a fitting parameter. At the large current densities and the low defect densities of interest the AN term is low and can be ignored. The other two terms, BN^2 and CN^3 dominate η_{rad}.

To increase η_{rad} one needs to increase the ratio of spontaneous emission rate over Auger recombination rate. Prior analysis of potential improvements in QW-based LEDs showed that standard methods to improve BN^2, such as non-c-plane crystal orientations or thinner quantum wells leads to improved wavefunction overlap and higher BN^2, but also a higher CN^3 [47]. An ideal solution would be one where the spontaneous emission rate is increased while the Auger recombination rate is decreased. This method is shown in Fig. 5b where the B coefficient is increased and C coefficient is decreased arbitrarily by factors of 10. Such changes in the two rates creates the expected large improvement in radiative efficiency and a shift of the PCE to higher current densities. We will show these changes in the recombination rates could be possible with QDs.

While the prospect of increasing spontaneous emission rate while decreasing Auger recombination rate is interesting, we need to determine if this is possible with QDs. First, we start with the spontaneous emission rate. The BN^2 term in Eqn. (10) can be replaced with the total spontaneous emission rate, R^t_{sp}, which is the integration of Eqn. (8) at various carrier densities. QD active regions are expected to have an advantage in spontaneous emission rates, because the increases observed in gain are translatable to R^t_{sp}. So, the higher density of states and wavefunction overlap also contribute to a higher spontaneous emission rate.

The change in the Auger recombination rate for QDs is a bit more complicated to determine. In Auger recombination, four states and three carriers participate in the process. The third particle (either electron or hole) receives the energy released from the recombination of the first two particles, promoting it to a higher energy state. Therefore, the bandstructure over a large k-space and large energy span needs to be accurately known. Once the bandstructure is determined, the states that satisfy energy and momentum conservation are used in Fermi's Golden Rule to estimate Auger recombination. Such calculations are difficult to undertake, difficult to determine validity, and are beyond the scope of this article.

To estimate Auger recombination rates in InGaN QDs we will leverage the sparse amount of literature on the subject. While it has been argued that the improved wavefunction overlap in InGaN QWs will not only lead to higher spontaneous emission but also Auger recombination [47], this may not be the case in InGaN QDs. Some theoretical work suggests the strong optical confinement in QDs will begin to limit the available states for the Auger carrier [28]. In fact, one argument is the recombination energy cannot be transferred to a bound energy state [27]. Therefore, if the energy barriers surrounding a QD are large enough, Auger recombination could be completely suppressed. While Ref. 27 did not consider III-nitride semiconductors, these barriers could possibly be accomplished with InGaN QDs using AlN or very high Al composition AlGaN barrier layers. Such theoretical predictions are compelling enough to warrant experimental verification.

There is some experimental work that suggests Auger recombination is decreased in semiconductor QDs, with Auger recombination rates of QDs from various materials decreasing with size [48], and smaller C coefficients measured for InGaN QDs [29]. In Ref. 29 a C_0 of $\sim 10^{-33}$ cm^6/s was measured, which is $\sim$100 times smaller than measured for InGaN QWs [4, 6]. As long as the decrease in Auger recombination rate is not accompanied with a similar decrease in spontaneous emission rates, then an increase in η_{rad} should be expected.

5. Efficiencies of InGaN QD-based light-emitting

We now compare the PCE of the SOTA QW-based LED [1] to a QD-based LED only considering the small QDs. Fig. 6 shows the total spontaneous emission rate (R^t_{sp}) for the QWs and QDs with increasing carrier density. The QDs have higher spontaneous emission at carrier densities of 10^{16}–10^{19} cm^{-3}. These carrier densities translate into current densities in the range of 0.05 – 3000 A/cm^2 using the chip areas and other recombination rates considered in this paper. The QDs have a more rapid increase in spontaneous emission at low carrier densities with an expected saturation at $\sim 5\times10^{17}$, similar to the gain. However, the LEDs can operate at higher carrier densities than LDs, and at $\sim 1\times10^{18}$ cm^{-3} there is a kink in the spontaneous emission curve due to carriers populating the second energy transition. This second transition is not considered as a parasitic recombination path because the produced photons can be used to pump phosphors, so it is included in the total spontaneous emission rate.

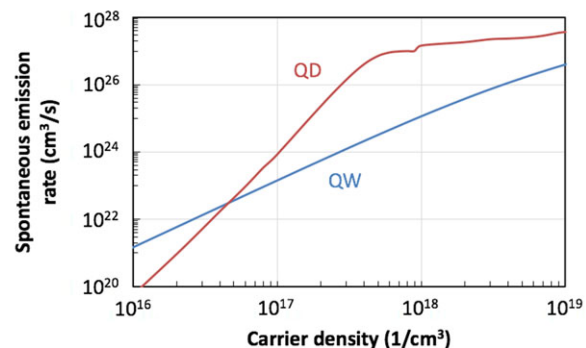

Figure 6 Plot of (a) spontaneous emission rate vs. carrier density for a QW (blue) and QD (red) active region. The QD active layer has higher spontaneous emission rates over the carrier densities of interest. The kink in the curve at $\sim 1\times10^{18}$ cm^{-3} is the onset of carrier filling in the second allowed transition.

© 2016 by WILEY-VCH Verlag GmbH & Co. KGaA, Weinheim

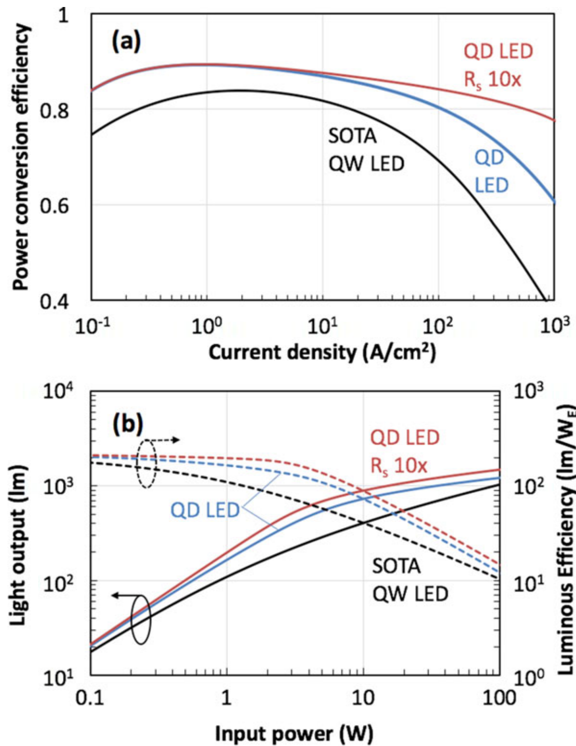

Figure 7 Plot of (a) power conversion efficiency vs. current density for a state-of-the-art (SOTA) QW LED (black line), a QD LED with increased spontaneous emission rate (QD LED, blue line), and a QD LED with an additional decrease in series resistance (QD LED R_s 10x, red line). The QD LEDs have improved efficiencies at high current densities. Plot of (b) the light output in lumens and luminous efficiency (lm/W$_E$) vs. input power for the same devices in (a).

We can now explore how the higher R^t_{sp} for QDs and different Auger recombination rates impact PCE. Fig. 7a shows the PCE versus current density for QD-based LEDs with various rates and the SOTA QW-based LED. The QD-based LEDs use the calculated R^t_{sp} while the SOTA QW-based LED uses the fitted BN^2. All the QD based LEDs have higher PCE, because of the higher spontaneous emission rate. For the QD LED (blue line) the C_0 coefficient is held constant at 10^{-30} cm^6/s, or raised and lowered by 10 times, and surprisingly all three Auger recombination rates produce the same PCE curve. This shows the high R^t_{sp} diminishes the effect of the Auger recombination rate. With high R^t_{sp}, the decrease in PCE at high current densities is now dominated by series resistance. The highest PCE curve (red line) includes an additional reduction in series resistance by 10 times. This analysis shows that if such QDs LEDs can be realized, series resistance will become the limiting factor in PCE.

The improvements in PCE will result in higher efficiency pc-LEDs. Fig. 7b shows the light output (lumens) and luminous efficiency (lm/W$_E$) versus input power from these sources. The QD-based LEDs have the desired higher luminous efficiency at higher input powers. The high efficiency curves suggest that 200 lm/W$_E$ could be achieved for

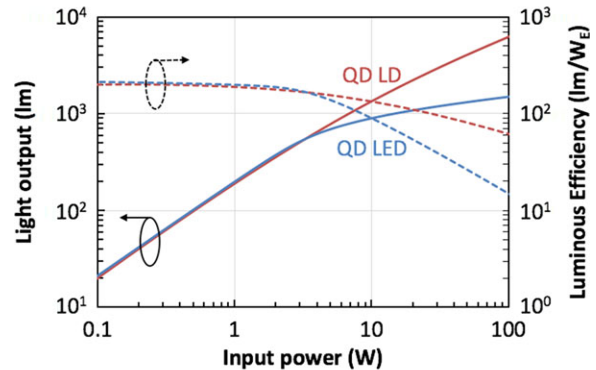

Figure 8 Plot of light output in lumens and luminous efficiency (lm/W$_E$) vs. input power for the best QD-based LDs and LEDs. The lumen output and efficiency is similar for the two devices up to 4 W. At higher powers the LD is more efficient and produces more lumens per device.

input powers up to 1 W, even without further improvementin series resistance. For the QD LED with low series resistance (red lines) ~500 lm at ~170 lm/W can be achieved at an input power of 3W. Surprisingly this is similar to the performance achieved by the QD-based LD shown in Fig. 4.

Finally, we compare the pc-LED and pc-LD results by plotting in Fig. 8 the phosphor-converted versions of the highest performing QD LD from Fig. 5 and QD LED from Fig. 7. With the improvements considered in this paper, the QD LED and LD have nearly similar performance at input powers from 0.1W – 4W. The performance diverges at 4W where the light output of both decrease because of series resistance, and the LD outperforms the LED. While there has been growing interest in lasers for SSL, this work suggests that QD active layers could also be very beneficial to LEDs, and maybe the best way to overcome Auger recombination. Of course, these calculations need to be verified with experimental data to determine validity. Subtle changes to the gain and spontaneous emission rates will change the PCEs for both the LD and LED.

6. Future research in InGaN quantum dots

The potential for high performance of QD-based LEDs and LDs make a compelling case for future investment in III-nitride QDs research. However, to achieve high performance in the modeling we used nearly ideal QDs with low inhomogeneous broadening (5 meV), small sizes (4 nm base width) and fairly high QD density (7×10^{10} cm^2). These parameters were chosen to ensure high gain and differential gain for LDs, and high spontaneous emission rate for LEDs. Such QDs are difficult to synthesize, not only in InGaN semiconductors, but in all semiconductors. Larger QDs and larger inhomogeneous broadening will only reduce performance. Therefore, to realize the QD-based LD and LED performance discussed above, we will need to devise ways to achieve nearly ideal QDs.

The most successful method to produce InGaN QDs is Stranski-Krastanov (SK) growth [49–51]. This synthesis

© 2016 by WILEY-VCH Verlag GmbH & Co. KGaA, Weinheim

method can produce QDs with enough gain for LD operation [31, 52], however the inhomogeneous broadening is large (~50-100 meV) and QD sizes can be large (up to 40 nm width). Additionally, the QD densities are modest at $\sim 3\text{-}4\times10^{10}$ cm^2. While this slightly lower density can be overcome by increasing the number of QD layers, confinement factors will decrease and detrimentally impact efficiency.

One potential method to create QDs with low inhomogeneous broadening, smaller QD sizes, and higher QD densities is quantum-sized controlled photoelectrochemical etching (QSC-PEC) [53–55]. In QSC-PEC, an initial QW or large-scale nanostructure is PEC etched using above-bandgap laser light for photoexcitation. Initially, the nanostructure absorbs the laser light, is oxidized by photoexcited holes, and etched by the electrolyte solution. As the nanostructure reduces in size from etching, the absorption edge blue-shifts due to quantum confinement. Ultimately, the QD can no longer absorb the laser light, resulting in a self-terminated etch at a precise final size that is determined by the laser wavelength. This approach results in controlled ensembles of QDs with low inhomogeneous broadening (PL FWHM = 6 nm), small sizes (width ~2.5 nm), and high QD densities ($\sim 1\times10^{11}$ cm^2) [56]. While this method is an interesting way to synthesize QDs, further development is necessary to ensure the QDs are not compromised by the etch process, and methods need to be devised to create multiple layers of QDs.

Further research is necessary to narrow or eliminate the gap between the properties of the today's uncontrolled experimental InGaN QDs (with large size distribution and low density) and the theoretically-predicted attractive properties of controlled QDs. SK growth has the longest research history, but has not yet produced QDs with the necessary controlled specifications. QSC-PEC is promising, but this method is new and there are many open questions that need to be researched to determine if it is a viable method. It is also very possible that some other method will be necessary. Clearly this is a challenging synthesis problem that warrants further investigation.

Finally, in the theoretical analysis we have assumed that the injection efficiency of the QD-based emitters is as high as the QW-based emitters. However, the QDs do not fill the entire injected area, and one could expect that carriers could be injected through the gaps in the QD layer. This is a problem for devices in other material systems and some solutions have been identified. One solution uses QWs within the device structure to capture carriers [57–59]. These carriers then are injected into the QDs via tunneling. Another possible solution is to increase the QD active volume by maximizing the fill factor of the QDs or increasing the number of QD layers to give the carriers enough chances to be captured within the QDs.

7. Summary

We have demonstrated that QDs are an attractive alternative to QWs, in both LEDs and LDs, to overcome Auger recombination and increase PCEs at higher input powers. In LDs, the QDs lead to lower threshold current densities, lower threshold currents, and higher PCEs. More specifically, we model threshold current densities of ~170 A/cm^2 and peak power conversion efficiencies of ~80%. In LEDs, the higher spontaneous emission rates lead to higher PCEs at higher current densities. Our modeling predicts peak power conversion efficiencies of 90% at low current densities (1 A/cm^2). Additionally, Auger losses are minimized and the decrease in power conversion efficiency at higher current densities is only due to resistive losses. When comparing the performance in phosphor-converted architectures, the LD and LED surprisingly perform similarly with luminous efficiencies of ~170 lm/W at an input power of 3 W. The challenge going forward is to find methods to synthesize QDs to meet the required sizes, inhomogeneous broadening, and densities. If successful, III-nitride light-emitting devices with QD active regions have the potential to outperform QW light-emitting devices, and enable an era of ultra-efficient SSL.

Acknowledgements. The authors would like to thank Ben Leung for his useful suggestions on the manuscript. Work at Sandia National Laboratories was supported by Sandia's Laboratory Directed Research and Development program. Sandia National Laboratories is a multiprogram laboratory managed and operated by Sandia Corporation, a wholly owned subsidiary of Lockheed Martin Corporation, for the U.S. Department of Energy's National Nuclear Security Administration under contract DE-AC04–94AL85000.

Received: 29 December 2015, **Revised:** 26 April 2016, **Accepted:** 2 May 2016

Published online: 26 May 2016

Key words: Quantum Dots, Solid-state lighting, light-emitting diodes, LEDs, laser diodes, LDs, efficiency droop, III-nitride, InGaN, GaN, phosphor-converted, PC-LEDs, Auger recombination.

References

[1] C. A. Hurni, A. David, M. J. Cich, R. I. Aldaz, B. Ellis, K. Huang et al., Appl. Phys. Lett. **106**, 031101–031105 (2015).
[2] J. Y. Tsao, M. H. Crawford, M. E. Coltrin, A. J. Fischer, D. D. Koleske, G. S. Subramania et al., Advanced Optical Materials **2**, 809–836 (2014).
[3] S. Nakamura and M. R. Krames, Opt. Express **101**, 2211–2220 (2013).
[4] Y. C. Shen, G. O. Mueller, S. Watanabe, N. F. Gardner, A. Munkholm, and M. R. Krames, Appl. Phys. Lett. **91**, 141101–141103 (2007).
[5] E. Kioupakis, P. Rinke, K. T. Delaney, and C. G. Van de Walle, Appl. Phys. Lett. **98**, 161107–161104 (2011).
[6] A. David and M. J. Grundmann, Appl. Phys. Lett. **97**, 033501 (2010).
[7] J. Iveland, L. Martinelli, J. Peretti, J. S. Speck, and C. Weisbuch, Phys. Rev. Lett. **110**, 177406–177405 (2013).
[8] J. J. Wierer Jr., J. Y. Tsao, and D. S. Sizov, Laser & Photonics Reviews **7**, 963–993 (2013).

© 2016 by WILEY-VCH Verlag GmbH & Co. KGaA, Weinheim

[9] K. J. Vampola, N. N. Fellows, H. Masui, S. E. Brinkley, M. Furukawa, R. B. Chung et al., Physica Status Solidi (a) **206**, 200–202 (2009).
[10] N. F. Gardner, G. O. Müller, Y. C. Shen, G. Chen, S. Watanabe, W. Götz et al., Appl. Phys. Lett. **91**, 243506 (2007).
[11] A. Laubsch, W. Bergbauer, M. Sabathil, M. Strassburg, H. Lugauer, M. Peter et al., Physica Status Solidi C **6**, S885–S888 (2009).
[12] Y. L. Li, Y. R. Huang, and Y. H. Lai, Appl. Phys. Lett. **91**, 181113 (2007).
[13] C. S. Xia, Z. M. SimonLi, Z. Q. Li, Y. Sheng, Z. H. Zhang, W. Lu et al., Appl. Phys. Lett. **100**, 263504 (2012)..
[14] D. A. Zakheim, A. S. Pavluchenko, D. A. Bauman, K. A. Bulashevich, O. V. Khokhlev, and S. Y. Karpov, Physica Status Solidi (a) **209**, 456–460 (2012).
[15] K. Kuramoto, A. Ohno, T. Yamada, H. Okagawa, and K. Kawasaki, 2007, Laser Review **35**, 69–72 (2007).
[16] S. Masui and S. I. Nagahama, Laser Review 2013, **41**, 899–904 (2014).
[17] U. Strauß, T. Hager, G. Brüderl, T. Wurm, A. Somers, C. Eichler et al., in: J.-I. Chyi, Y. Nanishi, H. Morkoç, J. Piprek, E. Yoon, and H. Fujioka (Eds.), Spie Opto, SPIE, 2014: pp. 89861L–10.
[18] J. J. Wierer Jr. and J. Y. Tsao, Physica Status Solidi (a) **212**, 980–985 (2015).
[19] J. J. Wierer, J. Y. Tsao, and D. S. Sizov, Physica Status Solidi C **11**, 674–677 (2014).
[20] R. Hasimoto, H. Hung, S. Saito, and S. Nunoue, Opt. Rev. **19**, 412–414 (2012).
[21] K. A. Denault, M. Cantore, S. Nakamura, S. P. DenBaars, and R. Seshadri, AIP Advances **3**, 072107 (2013).
[22] A. Lenef, J. Kelso, M. Tchoul, O. Mehl, J. Sorg, and Y. Zheng, in: M. H. Kane, J. Jiao, N. Dietz, and J.-J. Huang (Eds.), SPIE Optical Engineering + Applications, SPIE, 2014: pp. 91900C–11.
[23] J. J. Wierer, D. A. Steigerwald, M. R. Krames, J. J. O'Shea, M. J. Ludowise, G. Christenson et al., Appl. Phys. Lett. **78**, 3379–3381 (2001).
[24] O. B. Shchekin, J. E. Epler, T. A. Trottier, T. Margalith, D. A. Steigerwald, M. O. Holcomb et al., Appl. Phys. Lett. **89**, 071109 (2006).
[25] Y. Arakawa, Appl. Phys. Lett. **40**, 939–4 (1982).
[26] D. Bimberg, M. Grundmann, and N. N. Ledentsov, Quantum Dot Heterostructures, (John Wiley & Sons, 1999).
[27] J. L. Pan, Physical Review B **48**, 3978–3998 (2011).
[28] R. A. Abram, R. W. Kelsall, and R. I. Taylor, J. Phys. Chem. Solids **49**, 07–613– (1988).
[29] W. Guo, M. Zhang, P. Bhattacharya, and J. Heo, Nano Lett. **11**, 1434–1438 (2011).
[30] A. Banerjee, T. Frost, and P. Bhattacharya, Appl. Phys. Lett. **101**, 041108 (2012).
[31] T. Frost, A. Banerjee, K. Sun, S.-L. Chuang, and P. Bhattacharya, InGaN/GaN Quantum Dot Red (λ = 630 nm) Laser, **49**, 923–931 (2013).
[32] Y. R. Wu, Y. Y. Lin, H. H. Huang, and J. Singh, Appl. Phys. Lett. **105**, 013117 (2009).
[33] W. W. Chow and H. C. Schneider, Appl. Phys. Lett. **81**, 2566–2568 (2002).
[34] G. Liu, H. Zhao, J. Zhang, J. H. Park, L. J. Mawst, and N. Tansu, Nanoscale Res. Lett. **6**, 342 (2011).
[35] N. Tansu and L. J. Mawst, J. Appl. Phys. **97**, 054502 (2005).
[36] L. A. Coldren, S. W. Corzine, and M. L. Mashanovitch, Diode Lasers and Photonic Integrated Circuits, (John Wiley & Sons, 2012).
[37] T. Melo, Y.-L. Hu, C. Weisbuch, M. C. Schmidt, A. David, B. Ellis et al., Semicond. Sci. Technol. **27**, 024015–024017 (2012).
[38] S.-L. Chuang, Physics of Photonic Devices, (John Wiley & Sons, 2012).
[39] T. J. Bukowski and J. H. Simmons, Crit. Rev. Solid State Mater. Sci. **27**, 119–142 (2002).
[40] O. B. Shchekin, G. Park, D. L. Huffaker, and D. G. Deppe, Appl. Phys. Lett. **77**, 466–464 (2000).
[41] N. Kirstaedter, N. N. Ledentsov, M. Grundmann, D. Bimberg, V. M. Ustinov, S. S. Ruvimov et al., Electron. Lett. **30**, 1416–1417 (1994).
[42] K. Tachibana, T. Someya, and Y. Arakawa, Appl. Phys. Lett. **74**, 383–384 (1999).
[43] Nextnano software, Www.Nextnano.com. (n.d.). http://www.nextnano.com.
[44] B. Witzigmann, V. Laino, M. Luisier, U. T. Schwarz, H. Fischer, G. Feicht et al., IEEE Photon. Technol. Lett. **18**, 1600–1602 (2006).
[45] H. Zhao, G. Liu, J. Zhang, R. A. Arif, and N. Tansu, J. Display Technol. **9**, 212–225 (2013).
[46] A. David and M. J. Grundmann, Appl. Phys. Lett. **96**, 103504–103503 (2010).
[47] E. Kioupakis, Q. Yan, and C. G. Van de Walle, Appl. Phys. Lett. **101**, 231107–5 (2012).
[48] I. Robel, R. Gresback, U. Kortshagen, R. D. Schaller, and V. I. Klimov, Phys. Rev. Lett. **102**, 177404–4 (2009).
[49] F. Widmann, B. Daudin, G. Feuillet, Y. Samson, J. L. Rouvière, and N. Pelekanos, J. Appl. Phys. **83**, 7618–8 (1998).
[50] K. Tachibana, T. Someya, S. Ishida, and Y. Arakawa, J. Cryst. Growth **221**, 576–580 (2000).
[51] Y.-K. Ee, X.-H. Li, J. Biser, W. Cao, H. M. Chan, R. P. Vinci et al., J. Cryst. Growth **312**, 1311–1315 (2010).
[52] M. Zhang, P. Bhattacharya, and W. Guo, Appl. Phys. Lett. **97**, 011103–4 (2010).
[53] X. Xiao, A. J. Fischer, M. E. Coltrin, P. Lu, D. D. Koleske, G. T. Wang et al., Electrochim. Acta. **162**, 163–168 (2015).
[54] X. Xiao, P. Lu, A. J. Fischer, M. E. Coltrin, G. T. Wang, D. D. Koleske et al., J. Phys. Chem. C. (2015) acs.jpcc.5b09555.
[55] A. J. Fischer, J. Y. Tsao, J. J. Wierer Jr., X. Xiao, and G. T. Wang, US Patent 20150270136A1, n.d.
[56] X. Xiao, A. J. Fischer, G. T. Wang, P. Lu, D. D. Koleske, M. E. Coltrin et al., Nano Lett. **14**, 5616–5620 (2014).
[57] P. Bhattacharya, X. Zhang, Y. Yuan, K. K. Kamath, D. Klotzkin, C. Caneau et al., Optoelectronics and High-Power Lasers & Applications **3283**, 702–709 (1998).
[58] L. V. Asryan and S. Luryi, IEEE J. Quantum Electron **37**, 905–910 (9999).
[59] T. Chung, G. Walter, and J. N Holonyak, Appl. Phys. Lett. **79**, 4500–4502 (2001).

© 2016 by WILEY-VCH Verlag GmbH & Co. KGaA, Weinheim